



Impacts of Saharan dust as CCN on the evolution of an idealized tropical cyclone

Henian Zhang,¹ Greg M. McFarquhar,¹ Stephen M. Saleeby,² and William R. Cotton²

Received 2 March 2007; revised 30 May 2007; accepted 20 June 2007; published 28 July 2007.

[1] The impact of dust in the Saharan Air Layer (SAL) acting as cloud condensation nuclei (CCN) on the evolution of a tropical cyclone (TC) was examined by conducting simulations initialized with an idealized pre-TC mesoscale convective vortex (MCV) using the Regional Atmospheric Modeling System (RAMS). Increasing the background CCN concentration from 100 to 1000 and 2000 cm^{-3} in a layer between 1 and 5 km led to increases in averaged cloud droplet number concentration, and decreases in cloud droplet mean mass diameter through the entire simulation except during the initial spin-up. Dust in the SAL as CCN influenced the TC development by inducing changes in the hydrometeor properties, modifying the storm diabatic heating distribution and thermodynamic structure, and ultimately influencing the TC intensity through complex dynamical responses. The simulated storm intensities differed by up to 22 hPa depending on CCN concentration. The impact of CCN on storm intensity was sensitive to the background giant CCN (GCCN) vertical profile and presumably other environmental factors. The physical processes responsible for the impact of dust as nucleating aerosols on TC development need to be examined in the future under a wide range of environmental conditions.
Citation: Zhang, H., G. M. McFarquhar, S. M. Saleeby, and W. R. Cotton (2007), Impacts of Saharan dust as CCN on the evolution of an idealized tropical cyclone, *Geophys. Res. Lett.*, 34, L14812, doi:10.1029/2007GL029876.

1. Introduction

[2] During summer and early fall, intense heating over the Sahara desert forms a deep mixed atmospheric layer containing hot, dry air and mineral dust. As the air mass propagates westward over the Atlantic, it is undercut by cool, moist marine air. This elevated air mass is often referred to as the Saharan Air Layer (SAL). The SAL advances westward in association with the African Easterly Waves (AEWs), and it has frequently been observed to interact with tropical cyclones (TCs) within its vicinity [Dunion and Velden, 2004]. Hurricane Cindy (1999), Floyd (1999), Debby (2000), Joyce (2000), Felix (2001) and Erin (2001) are such examples. Dunion and Velden [2004] hypothesized that the SAL tends to suppress Atlantic tropical cyclone activity by introducing dry, stable air into the storm, increasing the vertical wind shear and enhancing

the temperature inversion at lower level. However, the additional role of dust in the SAL acting as cloud-nucleating aerosol on the storm development has yet to be determined.

[3] It is estimated that 240 ± 80 million tons of Saharan dust are transported from Africa to the Atlantic Ocean every year [Kaufman *et al.*, 2005]. Dust can directly impact the radiative balance of the earth by absorbing and scattering sunlight. Dust, especially those coated with sulfur and other soluble materials [Levin *et al.*, 1996], can also affect the cloud development by acting as cloud condensation nuclei (CCN), giant CCN (GCCN) and ice nuclei (IN) [DeMott *et al.*, 2003; van den Heever *et al.*, 2006]. Analysis of visible satellite imagery over the east Atlantic shows that the dust in the SAL can be drawn into nearby mesoscale convective systems, which can later develop into TCs. Hurricane Erin (2001) was one example. Although previous studies have shown that large numbers of dust particles can impact the development of shallow convective clouds, the role of CCN on the development of highly organized, strong convective systems such as TCs has not been thoroughly investigated. This study will examine the impact of dust acting as CCN on the initiation and evolution of a TC using numerical simulations.

2. Model Configuration

[4] To highlight the effect of dust as CCN, numerical simulations of a TC developing from an axisymmetric mesoscale convective vortex (MCV) in an idealized environment were conducted using the Regional Atmospheric Modeling System (RAMS) version 4.3 [Cotton *et al.*, 2003]. The simulations were initialized with the pressure, temperature and wind fields of an axisymmetric MCV consistent with observations obtained from several pre-TC MCVs [Montgomery *et al.*, 2006]. Three nested domains with horizontal resolutions of 24, 6 and 2 km were used. The numbers of horizontal grid points for Domain 1, Domain 2 and Domain 3 were 80×80 , 102×102 and 152×152 , respectively. There were 40 unevenly spaced vertical levels extending from the surface to 30 km with a minimum grid spacing near the surface of 300 m and a maximum vertical grid spacing of 1 km at higher altitudes. The Rayleigh friction absorbing layer extended from 20 km to 30 km. A sufficient depth of the Rayleigh friction absorbing layer and refined vertical resolution especially at higher altitudes are necessary to damp gravity waves so that they are not reflected downward as they can significantly affect the simulated storm intensity. The vortex was allowed to grow for 3 days in a zero wind environment over the ocean with a constant sea surface temperature (SST) of 29°C. Pre-TC MCVs are usually found on the southern edge of the SAL, which is a transient zone with hot and dry SAL air to the

¹Department of Atmospheric Sciences, University of Illinois at Urbana-Champaign, Urbana, Illinois, USA.

²Department of Atmospheric Science, Colorado State University, Fort Collins, Colorado, USA.

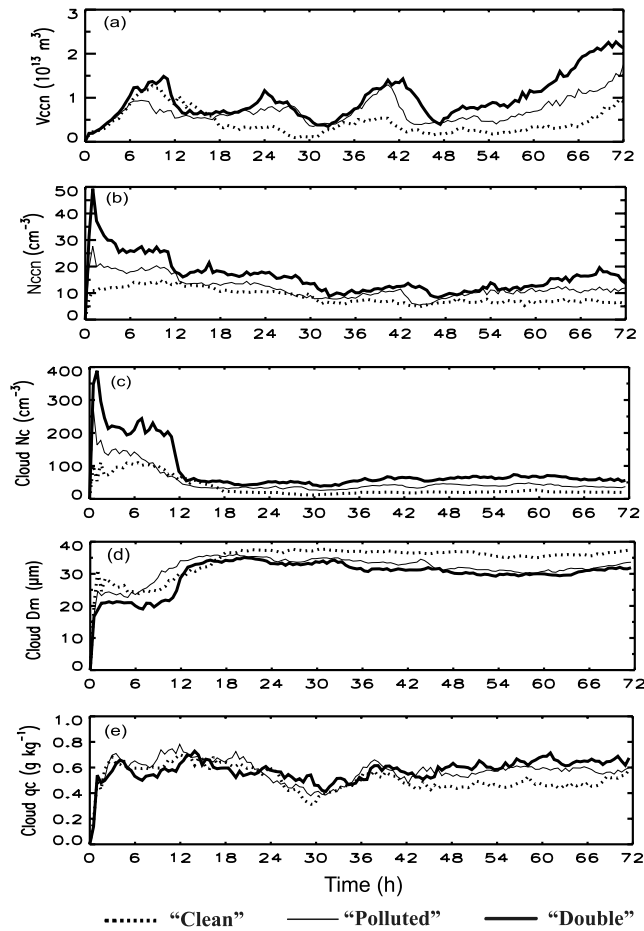


Figure 1. Temporal evolutions of (a) V_{ccn} , (b) N_{ccn} , (c) N_c , (d) D_m , and (e) q_c for “Clean” (dotted line), “Polluted” (thin solid line) and “Double” (thick solid line).

north and warm moist marine air to the south. Intrusion of dry air from the SAL into the convective systems could limit the impact of dust as nucleating aerosols. However, introducing this horizontal temperature gradient would require constructing an environmental wind field that satisfies the thermal wind balance and hence bring the impact of large scale wind shear into the simulations. Thus, to focus on the impacts of dust in the SAL acting as CCN, a horizontally uniform Jordan sounding [Jordan, 1958], which is likely a composite of soundings from both the SAL and non-SAL environments [Dunjon and Velden, 2004], was used.

[5] A two-moment microphysics scheme described by Cotton *et al.* [2003], which emulates bin microphysics for collection and sedimentation, was used in the simulations. Saleeby and Cotton [2004] described the extension of that scheme to include two modes of droplets and explicit activation of CCN and GCCN. The initial CCN distribution was horizontally homogeneous. Results from three sensitivity tests with different CCN vertical profiles representing clean, polluted and highly polluted scenarios are presented in detail. The clean simulation (hereafter “Clean”) was initialized with a constant CCN concentration of 100 cm^{-3} from the surface to 25 km. Dust particles were assumed to reside in a layer between 1 and 5 km [Karyampudi *et al.*, 1999]. To

represent elevated dust particles in the SAL, the polluted simulation (hereafter “Polluted”) was initialized with a CCN concentration of 1000 cm^{-3} between 1 km and 5 km. The double polluted simulation (hereafter “Double”) was initialized with a CCN concentration of 2000 cm^{-3} in the same layer. Since no direct measurement of a vertical profile of CCN over the ocean in the SAL was available, the CCN concentrations in “Polluted” were chosen based upon previous measurements in the dust plume [Levin *et al.*, 2005; van den Heever *et al.*, 2006]. The CCN concentrations at the surface and above 5 km in “Polluted” and “Double” were 100 cm^{-3} , by which a clean marine air layer was assumed to undercut the SAL. The CCN were further assumed to be mostly hydrophobic with a water solubility of 10% to represent desert dust particles coated with sulfate. The percentage of CCN activated during a time step depends upon temperature, vertical velocity, CCN median radius and number concentration [Saleeby and Cotton, 2004]. During the course of the simulation, CCN are advected, diffused, depleted through nucleation scavenging, and replenished through droplet evaporation.

[6] The initial background IN and GCCN concentrations were horizontally homogeneous. The IN concentration was 0.1 cm^{-3} from the surface to 20 km [van den Heever *et al.*, 2006]. The background GCCN concentration decreased from a maximum of 0.5 cm^{-3} at the surface to 0.08 cm^{-3} at 5 km and then reduced to zero at higher altitudes. To examine if the trends observed in the “Clean”, “Polluted” and “Double” are valid in general, an additional set of three simulations was performed using CCN concentrations that were identical to those described in “Clean”, “Polluted” and “Double”, but initialized with a different background GCCN profile. The GCCN profile had the same maximum value of 0.5 cm^{-3} at surface but was reduced to 0.01 cm^{-3} (instead of 0.08 cm^{-3}) at 5 km [van den Heever *et al.*, 2006]. Similarities and differences between both series of simulations are presented.

3. Results

[7] Figure 1 shows the time evolution of the total air volume having CCN activation (V_{ccn}), mean number concentration of activated CCN (N_{ccn}), mean cloud droplet number concentration (N_c), mean cloud droplet diameter (D_m), and mean cloud mixing ratio (q_c) for “Clean”, “Polluted” and “Double”. The cloud N_c , D_m , and q_c were averaged over the cloudy area in Domain 3. Figure 1a shows that, except for the first 18 hours when the model was initializing, CCN activation occurred in a greater volume of air if more ambient CCN were available even though the CCN activation maximum and minimum for the three simulations were not reached at the same time. The average N_{ccn} shown in Figure 1b was calculated by dividing the total number of CCN activated in Domain 3 by the corresponding V_{ccn} . The N_{ccn} averaged over the last 60 hours were 8.0, 10.6 and 13.9 cm^{-3} for “Clean”, “Polluted” and “Double”. This indicates that by increasing the background CCN concentration, more CCN were activated within a unit volume of air.

[8] The activated CCN number determines the number of cloud droplets formed through heterogeneous nucleation. The evolution of the total cloud droplet number closely

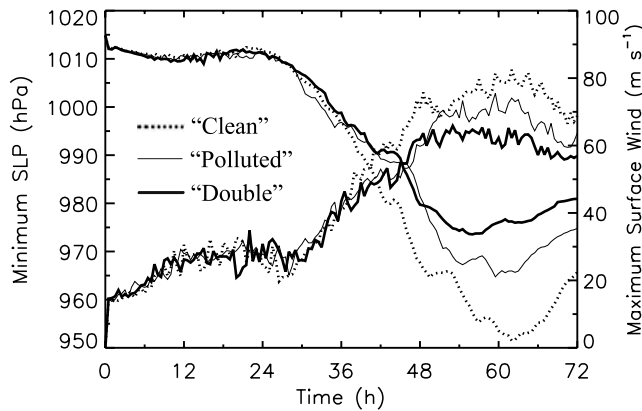


Figure 2. Temporal evolutions of the MSLP and maximum surface wind for “Clean”, “Polluted” and “Double”. Line types are the same as described in Figure 1.

followed the trend of total number of activated CCN with correlations of 0.91, 0.81 and 0.85 for “Clean”, “Polluted” and “Double”. Averaged over the last 60 hours, N_c for “Clean”, “Polluted” and “Double” were 22.6, 37.5 and 57.5 cm^{-3} , respectively (Figure 1c). “Clean” had larger cloud droplets with an average D_m of 36.2 μm compared to 33.7 and 30.6 μm for “Polluted” and “Double” (Figure 1d). The averaged q_c did not show a clear monotonic trend of increasing or decreasing with increasing CCN as did N_c and D_m until 46 hr (Figure 1e). The q_c may be significantly affected by factors such as updraft intensity, horizontal wind speed and moisture supply associated with the storm dynamics other than CCN concentration. Overall, Figure 1 shows that increasing the background CCN led to increases in V_{ccn} , N_{ccn} , N_c , and a decrease in D_m . The trends persisted through the entire simulation except during the initial spin-up.

[9] Varying CCN affected not only the cloud droplets but also the other hydrometeor categories (i.e., rain, ice, snow, aggregates, graupel and hail). To evaluate the sensitivity of the mean size, number concentration and total mass of all hydrometeor categories to CCN concentration, Mann-Whitney U tests were applied to determine which hydrometeor properties had statistically similar mean values for different simulations. For the following fields, the means of at least two simulations were different at a 95% confidence level: cloud droplet number, mass and diameter; rain drop number; ice number and mass; snow number, mass and diameter; aggregate number and diameter; graupel number and diameter; hail number and diameter. The CCN affected the other hydrometeor categories through a myriad of non-linear interactions occurring in the model. Differences in vertical profiles of the latent heating from diffusional growth, freezing, melting and evaporation were seen among the three simulations (figures not shown). The latent heating in turn modified the storm thermodynamic processes and affected storm structure, dynamics, and development.

[10] Figure 2 shows the temporal evolution of minimum sea level pressure (MSLP) and maximum surface wind for “Clean”, “Polluted” and “Double”. Three stages can be identified in the storm evolution: an initial stage from 0 to about 24 hr; a rapid intensification stage from 24 to about 60 hr; and a weakening stage from and after 60 hr. Figure 3 shows the surface radar reflectivity (Z) at 9, 60 and 70 hr for

the three simulations. 9 hr was about the time when the first CCN activation peaks were reached (Figure 1a). During the first 24 hours, small-scale cumulonimbus towers formed in regions with high absolute cyclonic vorticity and diabatic heating rates and grew by consuming ambient convective available potential energy (CAPE). They were referred to as the vortical hot towers (VHTs) by *Montgomery et al.* [2006]. Variations of diabatic heating rate distribution between simulations were observed as early as this initial VHTs forming stage. Figures 4a, 4c, and 4e show the azimuthally averaged diabatic heating rate at 9 hr for the three simulations. The diabatic heating in “Clean” was concentrated between 40 km to 60 km in the radial direction with an area having the maximum heating rates greater than 35 K hr^{-1} at 7.5 km above sea level. “Polluted” and “Double” showed less organized, less intense diabatic heating distributed over a broader radial distance with maximum heating rates not exceeding 20 K hr^{-1} , which is likely to be a result of azimuthally averaging since the diabatic heating in “Polluted” and “Double” showed less axisymmetry compared to “Clean” at this time. The total heating induced by the VHTs accumulated during the first 24 hours was not large enough to raise the temperature at the center of the vortex. Therefore the MSLP of all three simulated storms did not decrease (Figure 2).

[11] Between 24 hr and 36 hr, the VHTs gradually converged to the center of the MCV. The maximum surface wind speeds were greater than 20 m s^{-1} for all three simulations. Storms started to intensify rapidly through the wind-induced surface heat exchange (WISHE) process. The maximum storm intensity was reached around 60 hr with MSLP being 951.5, 964.7 and 973.6 hPa for “Clean”, “Polluted” and “Double”, respectively. Storm intensities differed by up to 22 hPa. By 60 hr, the storms resembled mature TCs for all three simulations. A tilted eyewall can be seen from the slopes in diabatic heating distributions at this time (Figures 4b, 4d, and 4f). As the strongest storm, “Clean” had the smallest eye and the widest eyewall (Figure 3b) with the highest diabatic heating rates of more than 140 K hr^{-1} (Figure 4b). Since the diabatic heating was concentrated in the eyewall around a small eye area, the eye of “Clean” was warmed up substantially by 60 hr with a maximum equivalent potential temperature (θ_e) of 397 K found at 4.7 km. As the weakest storm, “Double” had the biggest eye with maximum θ_e of only 374.9 K and a more asymmetric eyewall (Figure 3h) with diabatic heating rate up to only 40 K hr^{-1} (Figure 4f). The area with the heating rate greater than 20 K hr^{-1} within a radius of 45 km and 65 km corresponded to the spiral rainbands denoted by area with $Z > 50$ dBZ in Figure 3h. These rainbands propagated to the boundary of Domain 3 at 70 hr (Figure 3i). Spiral rainbands with $Z > 50$ dBZ also appeared later in “Clean” at 68 hr and “Polluted” at 63 hr. Their distributions at 70 hr can be seen in Figures 3c and 3f. Outward propagating rainbands associated with air of high potential vorticity (PV) tend to remove the PV from the core of TC, causing latent heat release away from the eyewall [*Guinn and Schubert, 1993*] and producing cold pools that inhibit further development of the eyewall. The occurrences of these spiral rainbands could be contributing to the weakening of the storms after 60 hr in these three simulations. Another factor that could contribute to the weakening of the storms is the

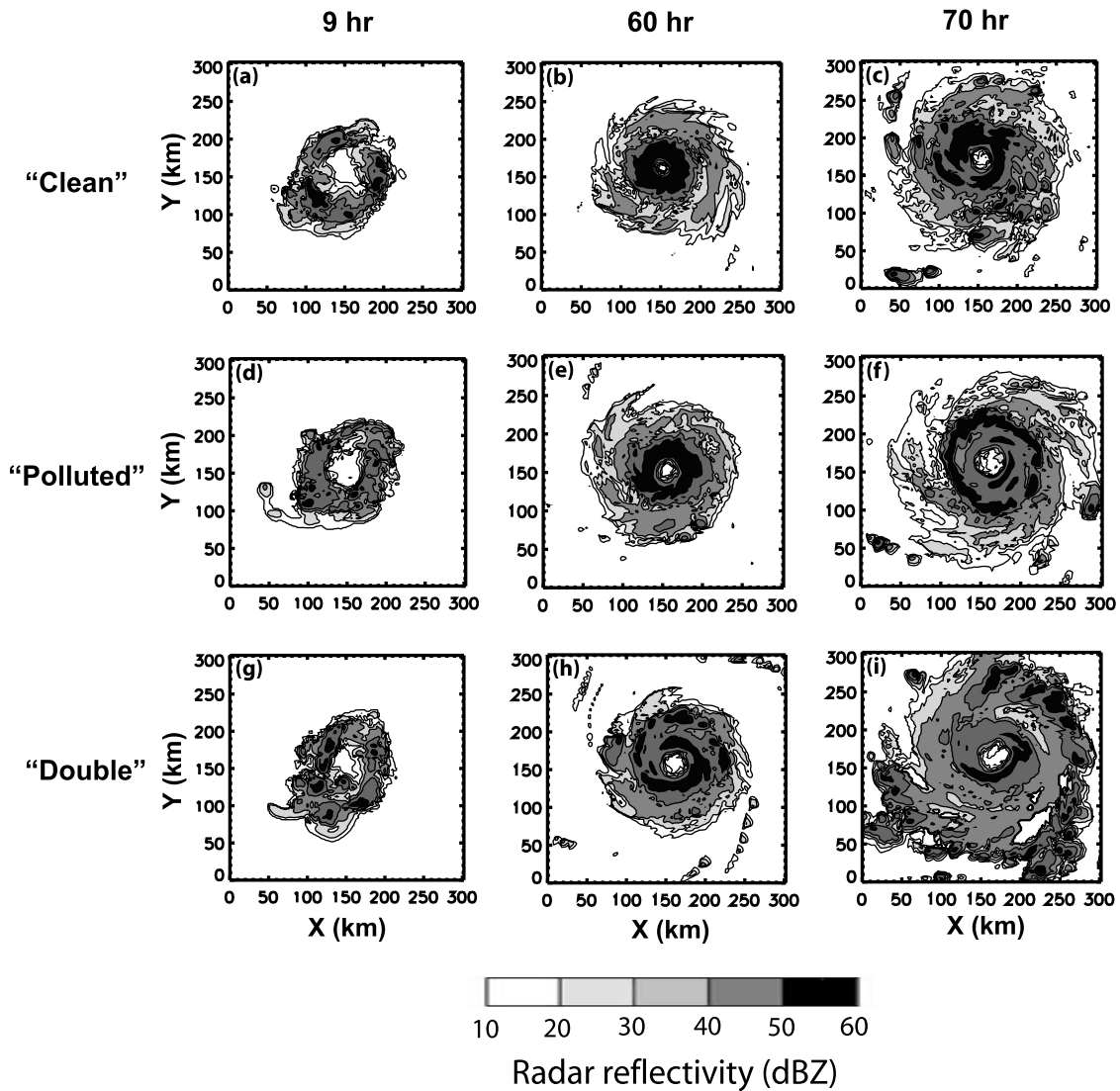


Figure 3. Surface Z at (left) 9 hr, (middle) 60 hr, and (right) 70 hr for (top) “Clean”, (middle) “Polluted” and (bottom) “Double”.

vertical wind shear induced by asymmetry of convection [Wu and Wang, 2000]. This wind shear also leads to the small displacements of storm centers up to 30 km from their original positions.

[12] During the 72 hours, the total precipitation reaching ground was 1.38 , 1.46 and $1.44 \times 10^{10} \text{ m}^3$ for “Clean”, “Polluted” and “Double” respectively. The difference of the total precipitation between simulations was less than 5% even though significant difference in the horizontal distributions of Z at 60 hr and 70 hr can be seen from Figure 3 when storms reached their mature stage.

[13] For the above three simulations, increased CCN led to increases in V_{ccn} , N_{ccn} , N_c , and a decrease in D_m with the difference in storm structure and diabatic heating distribution seen as early as the VHTs forming stage. These trends were consistently observed in the additional set of simulations with the same CCN profiles but with an alternate GCCN vertical profile as described in Section 2. However, the simple act of just changing the vertical GCCN profile did not result in a monotonic decrease of MSLP with increasing CCN. Simulated storms reached their maximum

intensity with MSLP of 970.3 hPa at 62 hr, 970.4 hPa at 71 hr and 966.5 hPa at 66 hr for simulations with CCN profiles as used in “Clean”, “Polluted” and “Double”, respectively. The simulation with initial CCN profile the same as “Polluted” was the weakest storm for 88% of the time after 30 hr. Although GCCN concentration is a small value compared to CCN concentration, GCCN could help to produce giant cloud droplets and affect the TC evolution by modifying the precipitation process and the latent heating distribution. The effect of CCN on TC intensity evolution can vary according to GCCN and presumably other environmental conditions. A more detailed analysis of the physical processes by which CCN and GCCN affected the development of the idealized TC will be presented in the future.

4. Discussion

[14] This paper presents evidence to show that dust as CCN may play a role in a TC’s development during its interaction with the SAL. The simulations of an idealized TC using the RAMS model initialized with a pre-TC MCV

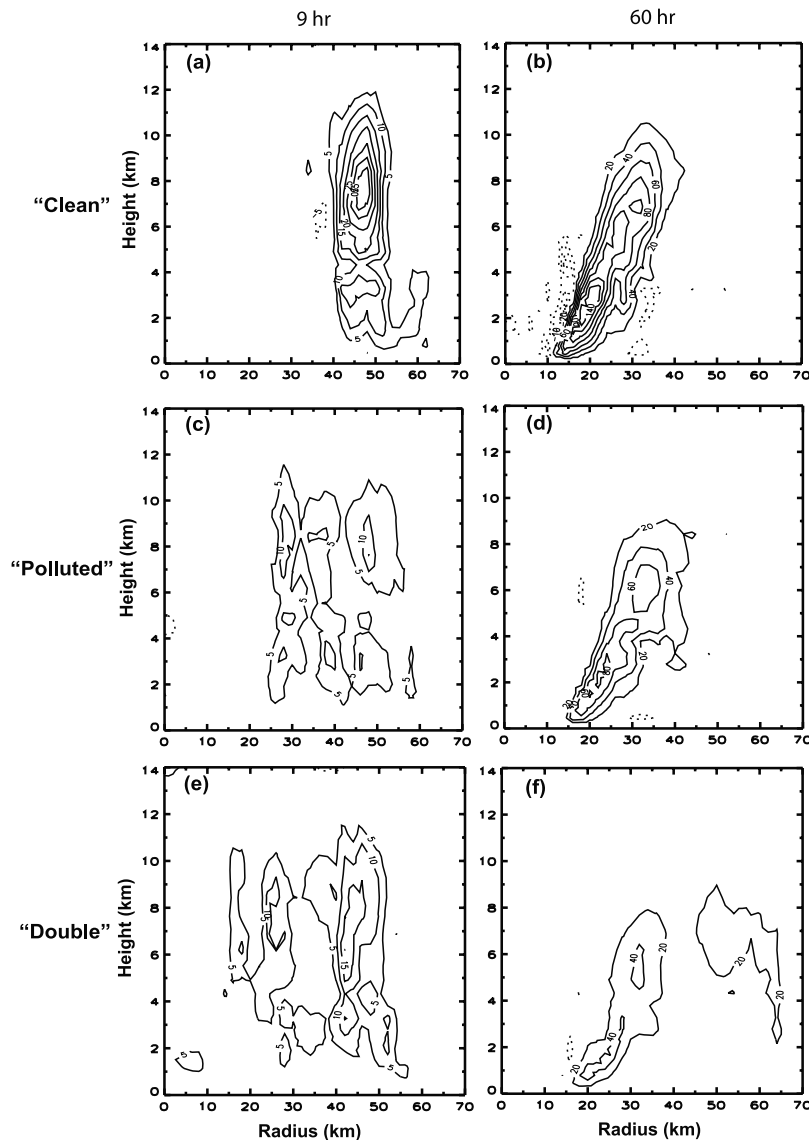


Figure 4. Azimuthally averaged diabatic heating rate (left) at 9 hr and (right) at 60 hr for (top) “Clean”, (middle) “Polluted” and (bottom) “Double”. Positive diabatic heating rates (solid lines) are contoured with an interval of 5 K hr^{-1} at 9 hr and 20 K hr^{-1} at 60 hr. Negative diabatic heating rates (dotted lines) are contoured with an interval of 5 K hr^{-1} at 9 hr and 10 K hr^{-1} at 60 hr.

have shown that dust in the SAL acting as CCN can influence TC development by inducing changes in the hydrometeor properties, modifying the storm diabatic heating distribution and thermodynamic structure, and ultimately influencing the TC intensity through complex dynamical responses. It has also been shown that the impact of varying CCN on storm intensity evolution is modified by other environmental conditions, such as the ambient GCCN concentration and its vertical profile. Ensemble simulations with combinations of various CCN, GCCN, and IN profiles under a variety of environmental conditions will be necessary in the future.

[15] In nature, relationships between CCN, GCCN and IN in SAL-TC systems are more complex than suggested by the idealized simulations presented here. Sea salt and other particles from evaporated sea spray generated by high winds are also significant sources of CCN and GCCN. The relative

importance of nucleating aerosols under various meteorological conditions, such as SST, wind shear and dry air intrusion, needs to be evaluated. Such impacts will need to be examined in a comprehensive coupled surface-ocean-atmosphere model under a wide range of conditions in the future.

[16] **Acknowledgments.** This work is supported by the NASA Earth System Science (ESS) Fellowship, grant NNG04GQ99H and the Tropical Cloud Systems and Processes (TCSP) mission, grant NNG05GR61G. The authors would like to thank M. Montgomery and M. Nicholls for providing the initial set up of the vortex, S. van den Heever for providing the reference IN and GCCN profiles, A. Loftus for the radar reflectivity calculation and B. Jewett for many useful discussions.

References

Cotton, W. R., et al. (2003), RAMS 2001: Current status and future directions, *Meteorol. Atmos. Phys.*, 82, 5–29.

- DeMott, P. J., K. Sassen, M. R. Poellet, D. Baumgardner, D. C. Rogers, S. D. Brooks, A. J. Prenni, and S. M. Kreidenweis (2003), African dust aerosols as atmospheric ice nuclei, *Geophys. Res. Lett.*, *30*(14), 1732, doi:10.1029/2003GL017410.
- Dunion, J. P., and C. S. Velden (2004), The impact of the Saharan Air Layer on Atlantic tropical cyclone activity, *Bull. Am. Meteorol. Soc.*, *85*, 353–365.
- Guinn, T. A., and W. H. Schubert (1993), Hurricane spiral bands, *J. Atmos. Sci.*, *50*, 3380–3403.
- Jordan, C. L. (1958), Mean soundings for the West Indies area, *J. Meteorol.*, *15*, 91–97.
- Karyampudi, V. M., et al. (1999), Validation of the Saharan dust plume conceptual model using Lidar, Meteosat, and ECMWF data, *Bull. Am. Meteorol. Soc.*, *80*, 1045–1074.
- Kaufman, Y. J., I. Koren, L. A. Remer, D. Tanré, P. Ginoux, and S. Fan (2005), Dust transport and deposition observed from the Terra-Moderate Resolution Imaging Spectroradiometer (MODIS) spacecraft over the Atlantic Ocean, *J. Geophys. Res.*, *110*, D10S12, doi:10.1029/2003JD004436.
- Levin, Z., E. Ganor, and V. Gladstein (1996), The effects of desert particles coated with sulfate on rain formation in the eastern Mediterranean, *J. Appl. Meteorol.*, *35*, 1511–1523.
- Levin, Z., A. Teller, E. Ganor, and Y. Yin (2005), On the interactions of mineral dust, sea-salt particles and clouds: A measurement and modeling study from the Mediterranean Israeli Dust Experiment campaign, *J. Geophys. Res.*, *110*, D20202, doi:10.1029/2005JD005810.
- Montgomery, M. T., M. E. Nicholls, T. A. Cram, and A. B. Saunders (2006), A vortical hot tower route to tropical cyclogenesis, *J. Atmos. Sci.*, *63*, 355–386.
- Saleeby, S. M., and W. R. Cotton (2004), Large-droplet mode and prognostic number concentration of cloud droplets in the Colorado State Univ. Regional Atmospheric Modeling System (RAMS). Part I: Module descriptions and supercell test simulations, *J. Appl. Meteorol.*, *43*, 182–195.
- van den Heever, S. C., G. G. Carrió, W. R. Cotton, P. J. DeMott, and A. J. Prenni (2006), Impacts of nucleating aerosol on Florida storms. Part I: Mesoscale simulations, *J. Atmos. Sci.*, *63*, 1752–1775.
- Wu, L., and B. Wang (2000), A potential vorticity tendency diagnostic approach for tropical cyclone motion, *Mon. Weather Rev.*, *128*, 1899–1911.

W. R. Cotton and S. M. Saleeby, Department of Atmospheric Science, Colorado State University, Fort Collins, CO 80523-1371, USA.

G. M. McFarquhar and H. Zhang, Department of Atmospheric Sciences, University of Illinois at Urbana-Champaign, Urbana, IL 61801, USA. (henian@atmos.uiuc.edu)